C. R. Mecanique 346 (2018) 26–38

Contents lists available at ScienceDirect

Comptes Rendus Mecanique

www.sciencedirect.com

The effect of indentation sequence on rock breakages: A study based on laboratory and numerical tests

Jie Liu [a,b,*], Jun Wang [a]

[a] Department of Building Engineering, Hunan Institute of Engineering, Xiangtan, China
[b] School of Resource, Environment and Safety Engineering, Hunan University of Science and Technology, Xiangtan, Hunan, China

ARTICLE INFO

Article history:
Received 18 June 2017
Accepted 14 November 2017
Available online 28 November 2017

Keywords:
Indentation sequence
Crack propagation
Stress evolution
Indentation efficiency

ABSTRACT

Rock may response differently to external loads applied in different sequences. Thus, we conducted indentation tests to investigate the effect of the indentation sequence on rock breakages. Sequential indentations, consuming less indentation energy, usually resulted in larger and deeper grooves and then led to lower specific energies. Thus, we conclude that sequential indentations occur instead of simultaneous indentations form larger grooves with the same indentation energy. To further validate this conclusion, we performed a series of numerical tests. The numerical analysis of stress evolution shows that, for simultaneous indentations, the propagation of an internal crack from an inner rim restrained the propagation of the other internal crack from the other inner rim. However, the chipping pattern varied for sequential indentations. In the first indentation process, an internal crack, initiating from an inner rim, is usually connected with an internal crack caused by the second indentation. The deflection angles of the internal cracks for the sequential indentations were smaller because of the lower compressive stress in the horizontal direction. Then, these smaller deflection angles led to larger chips.

1. Introduction

Indentation tests have been extensively applied to investigate the rock breakages that significantly affect indentation efficiency [1–3]. Specific energy (SE), determined by the chipping volume between indentations and the consumed indentation energy, is a critical index of cutting efficiency. Thus, extensive studies, applying single or multi indentations, have reported many important characteristics of chipping and indentation force. For the single indentation tests, Huang's theoretical investigation in plane conditions indicated that the initiation and deflection angles increase with the increase in confinements [4]. Simultaneously, the increase in confinements usually leads to increases in both indentation force and energy. In addition, the repeated indentations, conducted by a single TBM cutter on a soft rock, indicated that the preset indentation depth significantly affects rock breakages [5]. Then, the most unfavorable depth was obtained by analyzing the consumed energy and the chipping volume. Another numerical study, using single indentations, showed that shear failure occurs for small indentation depths, whereas tensile failure frequently occurs for larger depths [6]. Moreover, the numerical indentations by Gong indicated that joint spacing and orientation affect rock breakages, and thus further influence indentation efficiency [7,8]. Other studies, based on single indentations, have significantly contributed to understanding rock breakages [9,10]. However,

* Corresponding author at: Department of Building Engineering, Hunan Institute of Engineering, Xiangtan, China.
E-mail address: ljydslj@163.com (J. Liu).

https://doi.org/10.1016/j.crme.2017.11.004
1631-0721/

Table 1
Main mechanical parameters of the rock samples.

Mechanical parameters	Density (g/cm^3)	Elastic modulus (GPa)	Poisson's ratio	Uniaxial compression strength (MPa)	Tensile strength (MPa)	Friction angle (°)
Value	2.5	17.1	0.25	29.5	9.2	41.6

chips usually form between adjacent indentations; thus, rock breakages between indentations might be more representative. To investigate the rock breakages between indentations, extensive numerical tests in plane conditions have been conducted because of the analytic feasibility. Similarly, previous researchers investigated the effects of confinement, joint distribution and spacing–penetration (s/p) ratio on rock breakages. For instance, Ma proposed that the chipping level increases with an increase in confinement, when the confinement is higher than a critical value [11]. In addition, Bejari stated that indentation efficiency decreases with an increase in joint spacing for a specific orientation [1]. Moreover, based on the analysis of the consumed energy and of the chipping area, Moon proposed that the optimal s/p ratio is about 10 [12]. With other numerical studies [13,14], it has been concluded that crack propagation between adjacent indentations determines chip formation and thus further influences cutting efficiency. Accordingly, recent laboratory indentation tests have verified this conclusion. For example, simultaneous indentation tests showed that increased confinements may promote internal crack propagation between indentations [15]. Additionally, Liu's sequential indentation tests indicated that effective connections of the internal cracks are fundamental to the formation of deeper grooves between indentations, whereas insufficient connections of internal crack or poor incisions by surface cracks frequently result in shallow grooves with thin chips [16].

The above investigations show that many factors, such as confinements and s/p ratio, significantly affect crack propagation. However, the effect of the loading history, a factor affecting rock breakages, on crack propagation by indentations remains unknown. Thus, in the present article, we conducted simultaneous and sequential indentation tests on sandstone specimens for various s/p ratios and confinements. Additionally, we measured the groove morphology to study the rock breakage characteristics. To further investigate crack propagation between indentations, we conducted a numerical study based on PFC 2D.

2. Laboratory test

2.1. Test preparation

2.1.1. Rock sample preparation

Cubic sandstone specimens, whose length, thickness, and height were 25 cm, 20 cm, and 10 cm, were adopted in the present tests. According to the suggestions by the International Society of Rock Mechanics, the mechanical parameters in Table 1 were obtained by conducting uniaxial compressive, shear, and Brazilian tensile tests. Based on the classification by Yagiz [17] (Yagiz 2009), these specimens were of low brittleness. Specimens were incised from a big intact sandstone block; thus, the mechanical properties of the specimens are close. In addition, to ensure the even contact between rock surfaces and loading plates, the specimen surfaces were ground and lubricated before loading.

2.1.2. Test apparatus and design

To conduct simultaneous and sequential indentations, two kinds of indenters were adopted. Indenters (Indenter A), consisting of two semi-sized TBM blades with various spacings, were applied in the simultaneous indentation tests (Fig. 1(a)), whereas the indenter (Indenter B), containing a single semi-sized TBM blade, was applied in the sequential indentation tests (Fig. 1(b)). These indenters (high-temperature treated) were made of high-stiffness steel. In addition, the indenters were much stiffer than the specimens, thus, the deformation of the indenters in indentations is negligible. In addition, the same geometrical shape of each blade made the laboratory results comparable.

To practically simulate field indentations, these sandstone specimens were indented in biaxial states, achieved on a triaxial testing platform in Fig. 2(a). This platform consisted of a loading system, a controlling system, and a computer system. The high-stiffness loading frame made the indentation results reliable. Fig. 2(b) shows the free-body diagram of the rock specimen, placed in the loading chamber. Before indentation, the lateral surfaces of the specimen were compressed by servo-controlled horizontal forces to achieve specific confinements. The maximum and minimum confinements are denoted by <sigma>2 and <sigma>1, respectively. The differential stress that may significantly affect rock breakage is defined as <sigma>2-<sigma>1. Simultaneous and sequential indentations were conducted by applying the indenters in Figs. 1(a) and (b), respectively. In the indentation processes, the constant indentation rate (servo-controlled) was 0.5 mm/min; simultaneously, the computer system recorded and restored the indentation force and depth every few seconds. Then, the indentation energy was obtained by integrating the indentation depth and force. After indentation tests, to accurately measure the groove volumes formed between simultaneous or sequential indentations, the morphological measurement machine reported by Chen and Zhao was used [18,19]. Then, the groove morphology and volume were obtained by conducting the corresponding analyses.

Table 2 lists the specifications of two series of indentation tests. According to various s/p ratios and stress levels, the first and second series involved 6 and 8 indentation tests, respectively.

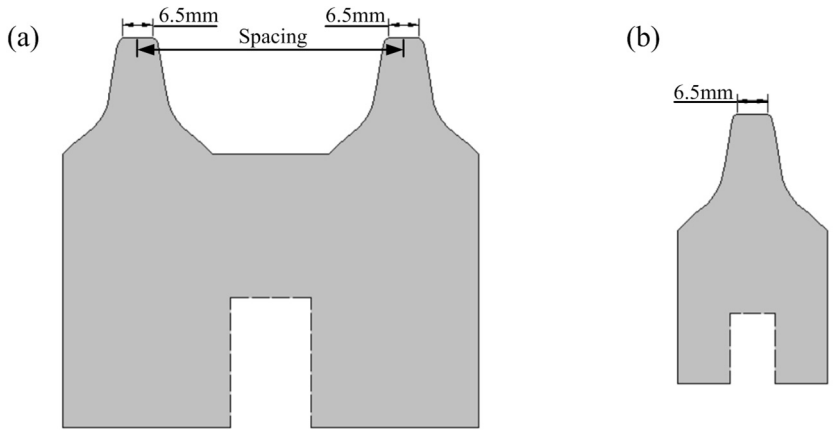

Fig. 1. Schematic diagram of the indenters.

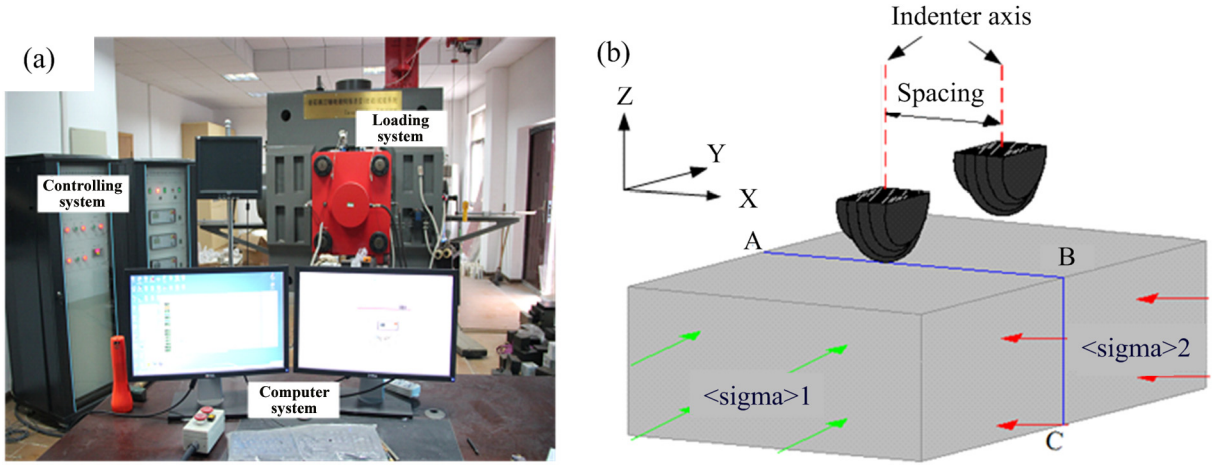

Fig. 2. Indentation test system and free-body diagram of the rock being indented.

Table 2
Detailed descriptions on indentation tests.

	Indenter used	Indentation rate (mm/min)	<sigma>2–<sigma>1 (MPa–MPa)	Spacing (mm)	Penetration (mm)	s/p
The first series	Indenter A and Indenter B	0.5	fixed	60, 70, 80	7.7	7.8, 9.1, 10.4
The second series	Indenter A and Indenter B	0.5	5–7.5, 5–10, 5–12.5, 5–15	70	9	7.8

3. Results and discussion

Groove volumes (influenced by chipping characteristics) and indentation energy (characterized by indentation forces) will determine indentation efficiency. Thus, in the following sections, we mainly investigate the chipping characteristics and indentation forces.

3.1. Chipping characteristics

Fig. 3 shows the typical rock breakages caused by sequential and simultaneous indentations for spacing and indentation depth of 60 mm and 7.7 mm in the first series of tests. Fig. 3(a1) indicates that a big chip, denoted by a dash line, formed at the shallow part after the first indentation. After the second indentation, fierce rock breakages, characterized by the chip formation at deeper parts, subsequently occurred (Fig. 3(a1)). Similarly, relatively fierce incisions by surface cracks occurred. These incisions led to the formation of small chips after the simultaneous indentations (Fig. 3(b1)). After the removal of the chips, on the groove surfaces in Figs. 3(a2) and 3(b2), the traces of the propagated surface cracks, denoted in black dash lines, indicate that the surface crack incised the rock between indentations. This phenomenon agrees well with previous studies [16]. The denser traces of surface cracks in Fig. 3(b2) infer that fiercer surface crack incisions occur for simultaneous

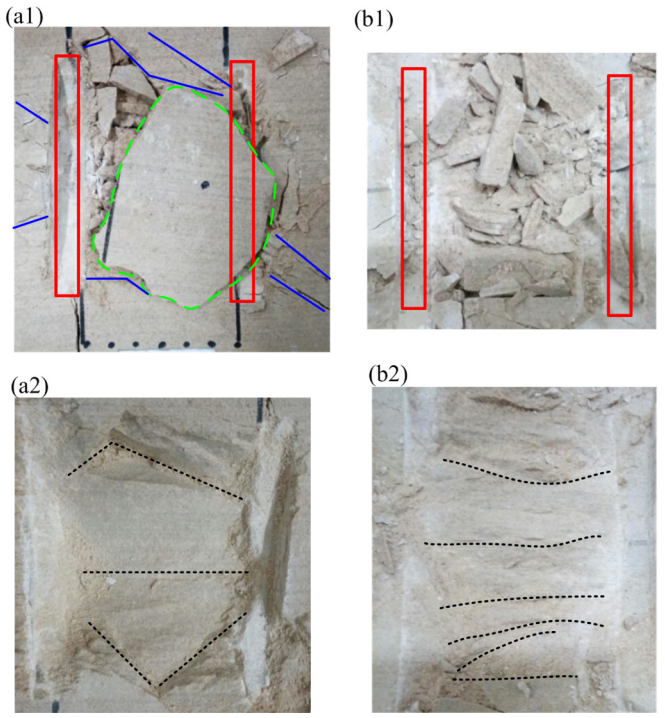

Fig. 3. Rock breakages for sequential and simultaneous indentations: (a1) and (b1) are the rock breakages after sequential and simultaneous indentations; (a2) and (b2) are the groove surfaces after the removal of the chips.

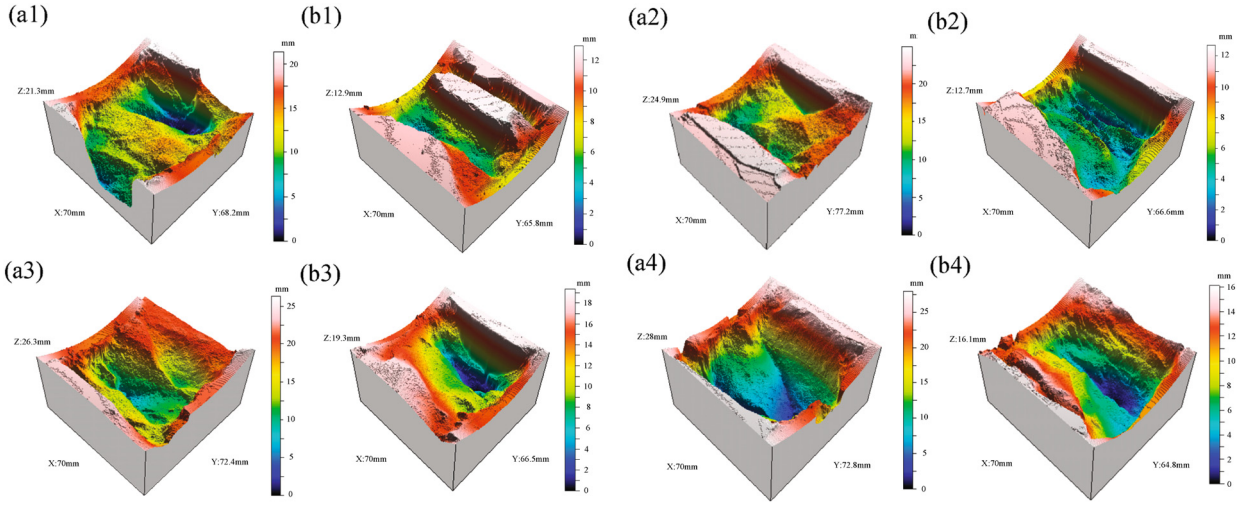

Fig. 4. Groove morphologies for sequential and simultaneous indentations in the second series of tests: (a1) and (a2) are the groove morphology for sequential indentation tests; (b1) and (b2) are the groove morphology for simultaneous indentation tests.

indentations. Nevertheless, the measurement on these two grooves indicates that the maximum depth for sequential indentations was larger. We observed similar phenomena in the other tests. For instance, in the second series of indentation tests, when the stress level (<sigma>1–<sigma>2) was 5 MPa–7.5 MPa, Fig. 4 shows that the maximum groove depth was 21.3 mm after two sequential indentations; however, the corresponding maximum depth was only 12.9 mm for the simultaneous indentations. With the increases in <sigma>2, the maximum depths for sequential indentations increased, whereas a smaller variation occurred for the simultaneous indentations. Thus, it can be concluded that, for the same indentation conditions, the maximum depth for sequential indentations is larger than that for the simultaneous indentations. With Liu's conclusions and the rock breakage characteristics in Fig. 3 [16], we further conclude that more effective connections of internal cracks at deeper parts of the rock specimen occur for sequential indentations instead of simultaneous indentations.

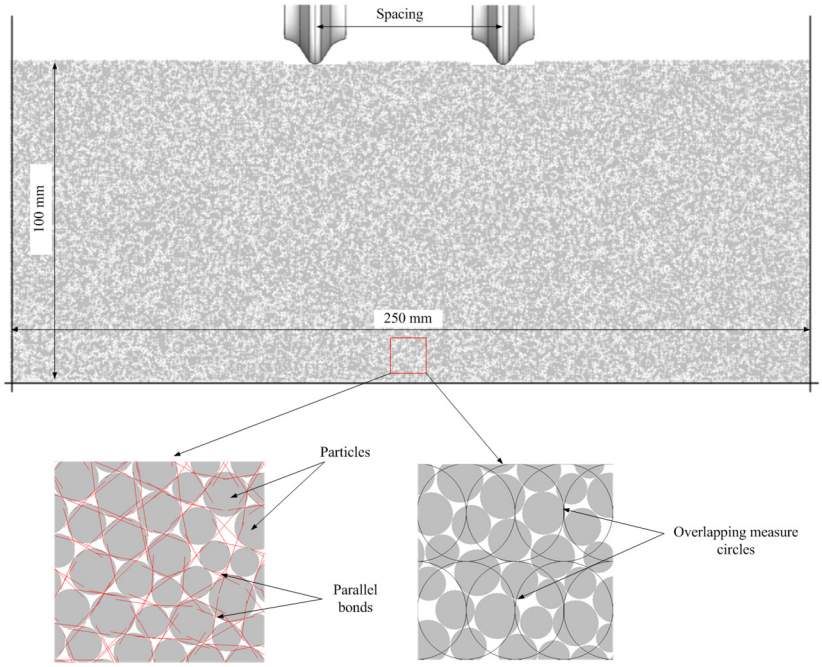

Fig. 5. Indentation model.

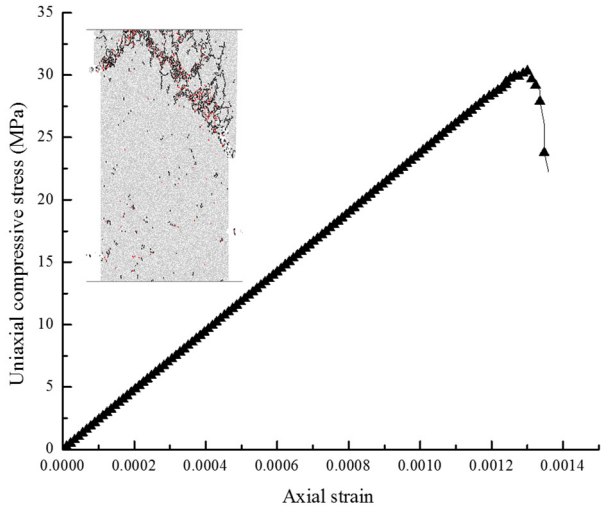

Fig. 6. Calibration of the uniaxial compressive strength.

To investigate how sequential indentations promote internal crack connection at deeper parts, we conducted several numerical tests to simulate the first series of indentation tests in Table 2 using PFC 2D, a commercial software that has been widely used to investigate the rock failure process [20]. Fig. 5 shows the details of the numerical model, consisting of 41,285 particles, 105,884 parallel bonds and 5 walls. In addition, 10,000 measure circles with a radius of 1 mm were installed to monitor stress conditions every few steps. Before indentations, to make numerical and laboratory tests comparable, we calibrated the uniaxial compressive strength of the model (Fig. 6). The calibrated uniaxial compressive strength (30.3 MPa) was close to that of the sandstone specimen applied in the present article. The micro- and macro-parameters are listed in Table 3.

Fig. 7 shows crack propagation caused by simultaneous and sequential indentations. For simultaneous indentations, an internal crack initiated from a plastic zone and approximately connected the adjacent plastic zones (Figs. 7(a1)–(a3)). However, for sequential indentations, two internal cracks, initiating from two plastic zones, completely connected two plastic zones and thus formed large chips. Additionally, larger chips, resulted from sequential indentations instead of simultaneous indentations, formed at deeper parts. The typical crack propagation in the laboratory, obtained by incising the specimen

Table 3
Micro and macro synthetic parameters.

Micro-parameters	Values	Macro parameters	Value
Minimum radius (mm)	0.32	Uniaxial compression stress, UCS (MPa)	30.3
R_{max}/R_{min}	1.66		
Particle contact modulus (GPa)	9.5		
Particle normal/shear stiffness	2.5	Young's modulus, E (GPa)	2.3
Friction coefficient	0.5		
Parallel bond modulus (GPa)	9.5		
Parallel normal/shear stiffness	2.5	Poisson ratio	0.22
Parallel bond normal strength (MPa)	17.7		
Parallel bond shear strength (MPa)	19.8		

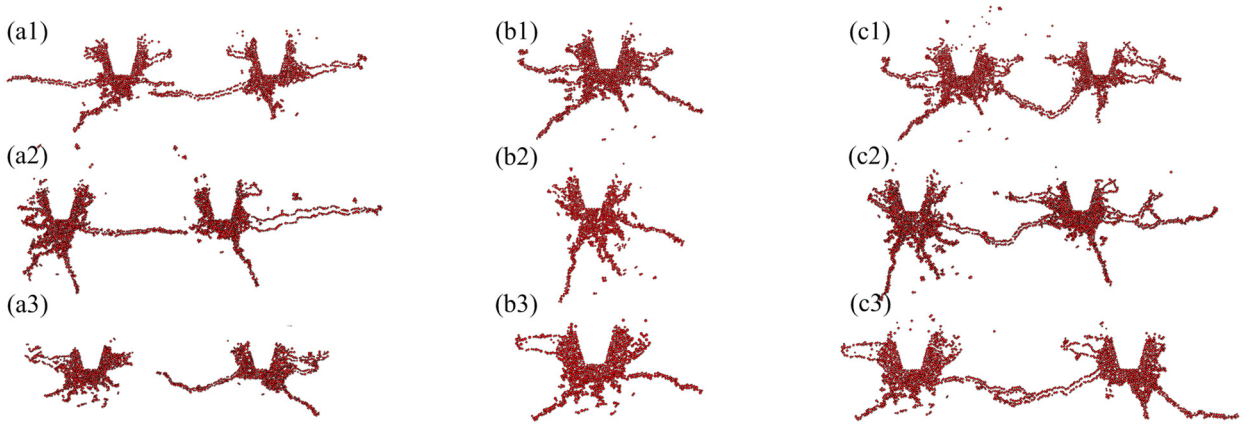

Fig. 7. Crack propagation for different indentation modes: (a1)–(a3) are the crack propagation for spacings of 60 mm, 70 mm, and 80 mm after simultaneous indentations; (b1)–(b3) are the crack propagation for spacings of 60 mm, 70 mm, and 80 mm after the first indentation; (c1)–(c3) are the crack propagation for spacings of 60 mm, 70 mm and 80 mm after the second indentation.

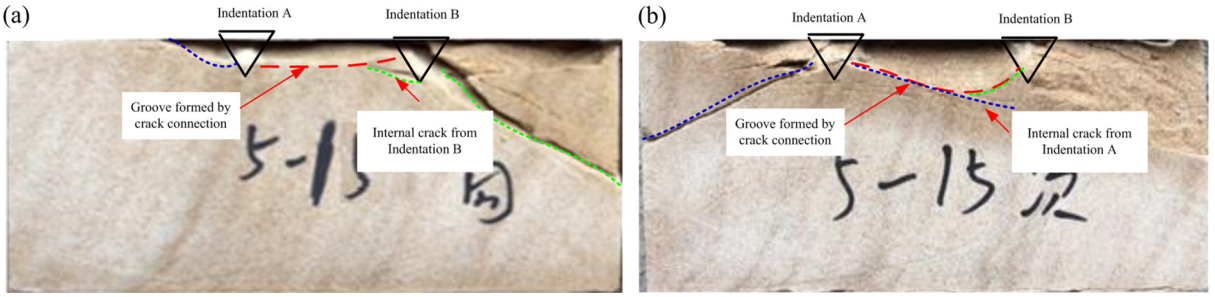

Fig. 8. Typical crack propagation in the second series of tests for a stress level of 5–15 MPa: (a) simultaneous indentations; (b) sequential indentations.

along the ABC plane in Fig. 2(b), agrees well with these phenomena. The groove outline in Fig. 8(a) indicates that the groove may form by internal crack propagation of only one internal crack, though a crack, denoted by a green dash line, initiated from indentation B and connected with the groove outline. In contrast, for sequential indentations, after the first indentation, an internal crack in the blue dash line formed (Fig. 8(b)). Then, the outline of the groove, denoted by a red dash line, may form by internal crack connection after the second indentation.

We believe that the stress conditions in the indentation process are responsible for the variation of crack connections. Thus, the following section mainly analyzes the maximum principle stress that is the impetus for crack propagation [21].

Fig. 9 depicts crack propagation and the evolution of the maximum principle stress in the simultaneous indentation process in Fig. 7(a1). In PFC 2D, the tensile stress is positive [22]. Clearly, the cores of the tensile stress concentrations overlapped with crack tips. Thus, it can be concluded that the concentrated tensile stress is responsible for crack propagation. In addition, before the initiation of the internal crack that approximately connected two adjacent plastic zones, a highly tensile concentrated zone formed near the right inner rim (Fig. 9(a)). Simultaneously, a concentrated zone, with slightly lower tensile stress, formed at the left inner rim. When the indentation depth increased to 6.6 mm, the internal crack from the right rim slightly propagated; simultaneously, the tensile stress concentration at the crack tip also gently diminished. In contrast, the internal crack from the left inner rim failed to propagate, but the tensile stress concentration at the crack tip significantly dissipated. With further increases in the indentation depth, the internal crack from the right inner rim con-

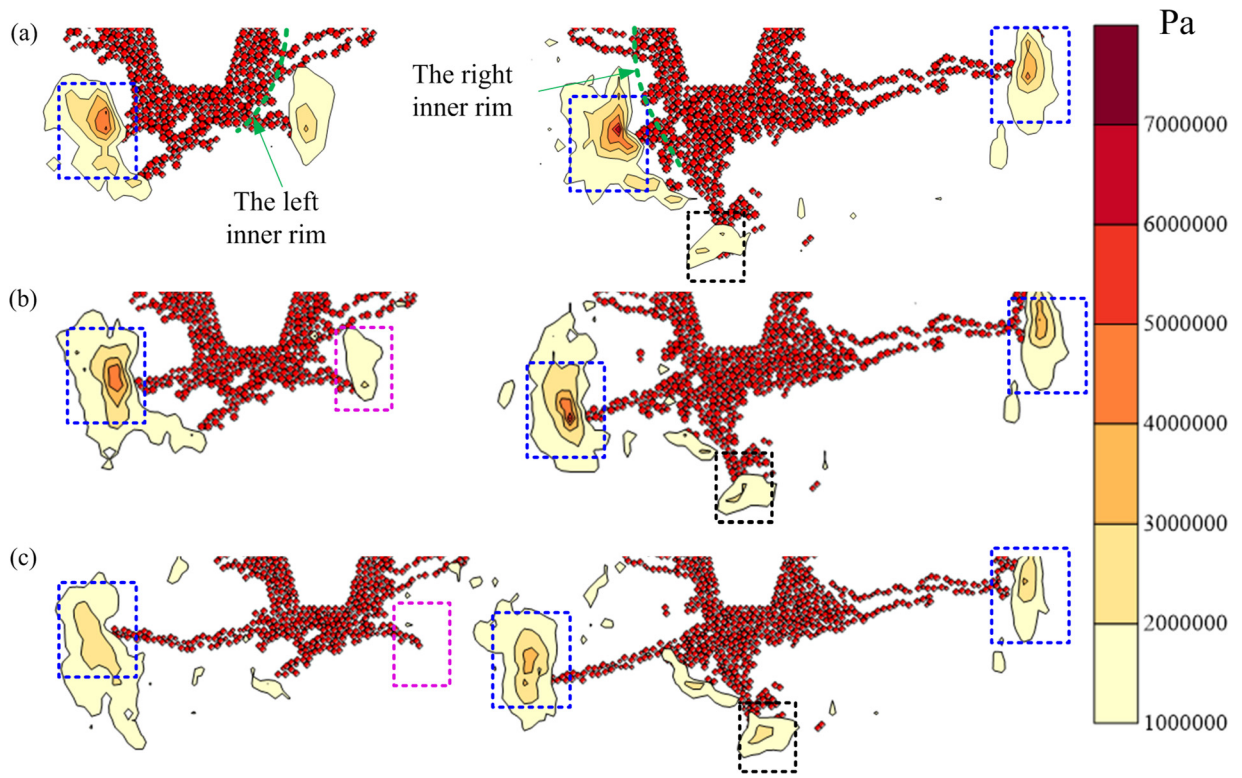

Fig. 9. Crack propagation and the contour of the maximum principle stress for various indentation depths: (a), (b) and (c) correspond to 6.2 mm, 6.6 mm, and 7.0 mm, respectively.

tinuously propagated; however, the left one failed to propagate because of the dissipated tensile stress concentration. Thus, we can preliminarily infer that the dissipated tensile stress concentration is responsible for the cease of the propagation of the left internal crack. Nevertheless, the cause of the dissipation of the tensile stress remains unknown. Two kinds of crack propagation, propagation of internal cracks from the same plastic zone and propagation of internal cracks from the other plastic zone, may be responsible for that.

Fig. 9 indicates that three internal cracks, enclosed in blue rectangles, propagated in the indentation process. In addition, the concentrated tensile stress at these crack tips dissipated in the propagation process. For the right indentation, crack propagation resulted in the tensile stress concentration (enclosed by black rectangles) at another crack tip that ceased to propagate. However, for the left indentation, tensile stress dissipation at the crack tip, which ceased to propagate, also occurred. Thus, it seems that the results of the effect of crack propagation on the tensile stress concentration at the other crack tips conflict. In the following discussion on sequential indentation tests, we will further discuss this phenomenon.

Fig. 10 depicts two typical crack propagation processes in the first indentation process. The tensile stress concentrations and the crack propagation are enclosed in blue rectangles. The promoted tensile stress concentrations, enclosed in black rectangles, agree well with the phenomenon observed from the right indentation in Fig. 9. Thus, we can infer that internal crack propagation frequently leads to the tensile stress concentrations at the tips of the other cracks that cease to propagate. Thus, the dissipation of the tensile stress concentration, enclosed in pink rectangles in Fig. 9, may result from the continuous propagation of the internal crack from the right inner rim. Therefore, for simultaneous indentations, the chipping pattern in Fig. 7, characterized by the connection of only one internal crack, has been verified.

For sequential indentations, the internal crack, caused by the second indentation, is connected with the internal crack induced by the first indentation (Fig. 7). The stress evolution in Fig. 11 may shed light on this phenomenon. After the first indentation, the first internal crack, connecting two plastic zones, ceased to propagate (Fig. 11). Thus, we monitored the stress conditions at the tip of this internal crack. At the early stage of the second indentation, compression at the tip first accumulated. When the indentation depth for the second indentation increased to about 0.3 mm, the maximum principle stress increased. This increase led to the compression dissipation at the tip. With further increase in the indentation depth to about 0.8 mm, the maximum principle stress was zero. When the indentation depth continued to increase, both the maximum principle stress and the minimum principle stress significantly increased. The positive maximum principle stress indicates that a tensile concentration zone formed at the crack tip. Zhang's study indicated that cracks frequently propagate towards the less compressed zones [23]. Similar phenomena have also been reported by Zhai and Liu [13,24]. Thus, the dissipation of the compressive stress at the tip results in the connection of the cracks from adjacent plastic zones.

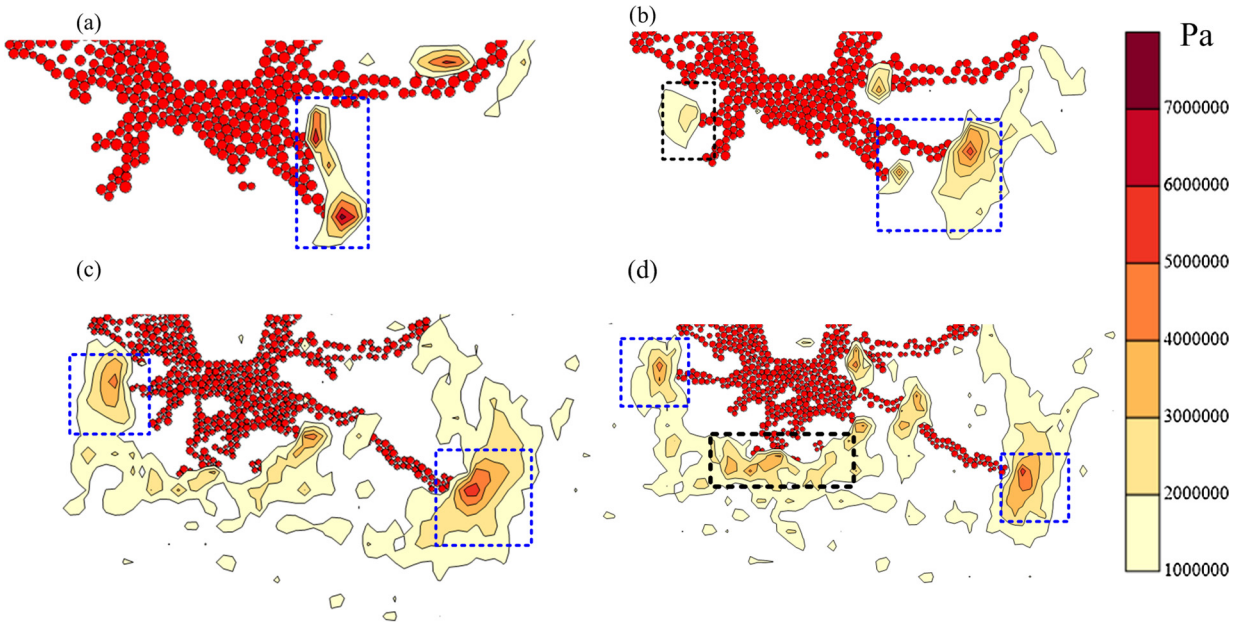

Fig. 10. Crack propagation and stress concentrations for various indentation depths in the first indentation process: (a), (b), (c), and (d) correspond to 3.6 mm, 4.0 mm, 4.8 mm, and 5.2 mm.

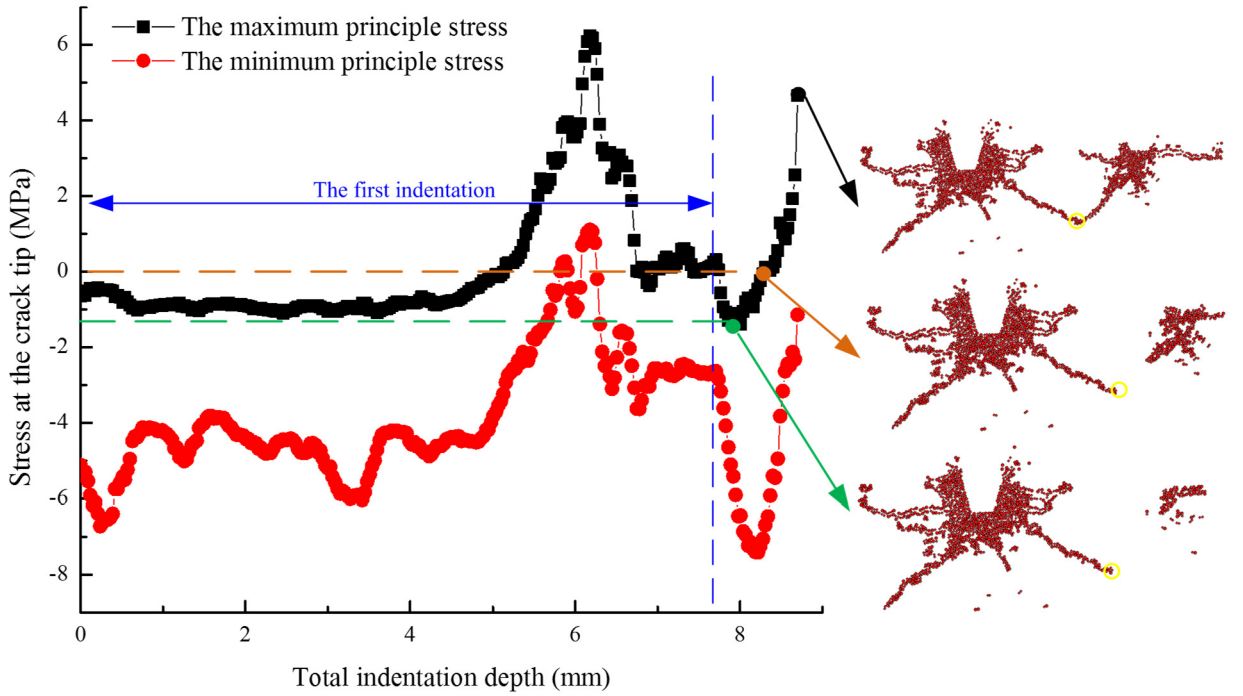

Fig. 11. Monitored stress conditions at the crack tip denoted by a yellow circle.

The above numerical study indicates that chips form by internal crack propagation. In addition, the initiation angle (α) and the deflection angle (β) in Fig. 12(a) will determine the chip shape and size and thus further influence indentation efficiency. Thus, we measured the average α and β values of the internal cracks, connecting two plastic zones. Clearly, the indentation sequence slightly influenced the initiation angle (Fig. 12(b)). In contrast, sequential indentations usually resulted in smaller deflection angles and then further led to larger chips. However, the cause of the propagation difference remains unknown.

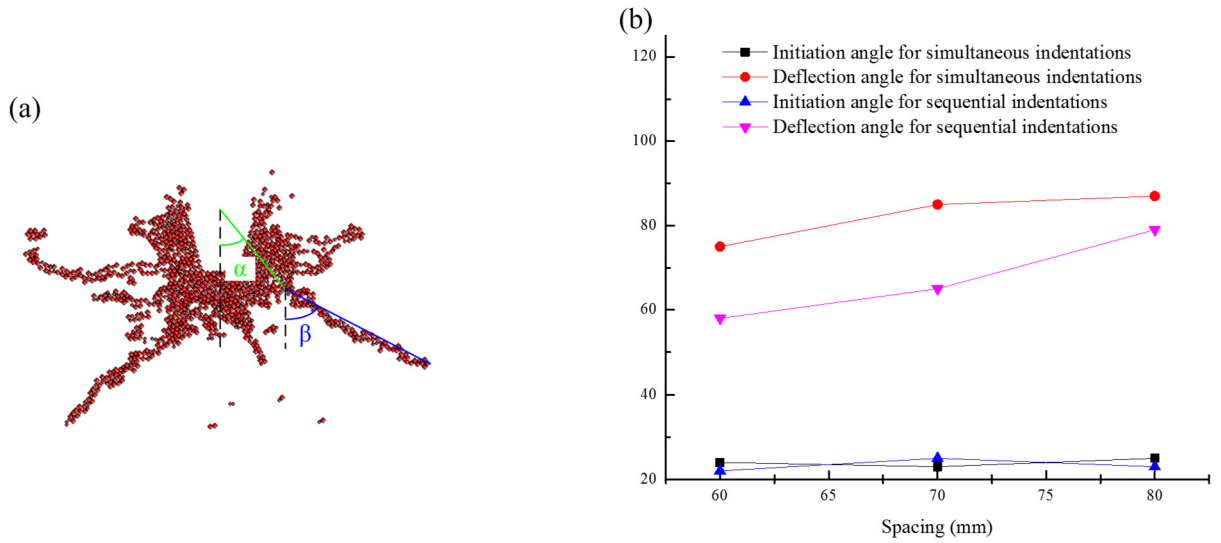

Fig. 12. Definition of the internal crack and measured initiation and deflection angles.

Previous studies indicated that the maximum compressive stress may determine the crack propagation trajectory [25,26]. Thus, we investigated the horizontal compressive stress between indentations that may affect the crack propagation direction. Before crack initiation, Fig. 13 depicts contours of a ratio, obtained by dividing the horizontal stress in the simultaneous indentation by that in the sequential indentation test. The black curves, enclosing the brown and pink initiation points, indicate that the ratio was higher than 4 before crack initiation. In other words, compared to sequential indentations, higher horizontal stress was induced for simultaneous indentations. Previous studies proposed that cracks propagate along the trajectory of the maximum compressive stress [25,26]. In addition, according to Griffith's theory, when the strength of the rock is reached at crack tips, the cracks extend. The crack propagation energy is the strain energy release rate, G_C [12,27].

The fracture criterion for the internal crack is [28]:

$$G_C = \frac{K_I^2}{E} + \frac{K_{II}^2}{E} \tag{1}$$

E is the elastic modulus of the rock specimen, and K_I and K_{II} can be written as [28]:

$$K_I = \sigma_t^{\frac{3}{2}} \sqrt{\pi} F \tag{2}$$

$$K_{II} = 0.5\sigma\,[f\alpha^2 + \sin\alpha - 2f]\sqrt{\pi a} \tag{3}$$

where G_C is the critical strain release rate, σ_t is the maximum tensile stress, F is a constant determined by the size of minor cracks, α is the initiation angle, f is the friction coefficient on the crack surfaces, a is the length of the crack, σ is the horizontal stress.

The deflection angle β is determined by the following equation [28]:

$$K_I \sin\beta + K_{II}(3\cos\beta - 1) = 0 \tag{4}$$

According to Eq. (4), the previous study indicated that the increase in σ (the horizontal stress in the present article) leads to the increase of deflection angle, β [15]. Thus, the higher compressive stress in the horizontal direction, induced by simultaneous indentations, will result in larger deflection angles (Fig. 12(a)), and the curved crack may approximately propagate along the horizontal direction. This conclusion agrees well with the results in Fig. 12(b).

3.2. Characteristics of the indentation forces

Fig. 14 shows the typical indentation forces that determine indentation energy. For simultaneous indentation tests, the indentation force increased with the increase in indentation depth at stage A, the pre-peak stage. When the depth increased to about 5.5 mm, the indentation force peaked at 510 kN. With further increase in indentation depth, the fluctuation of the indentation force occurred at stage B, the post-peak stage. Previous studies indicated that these fluctuations may result from crack propagation in rock specimens [14,16]. For the first indentation in the sequential indentation tests, a similar increase in the indentation force was observed before the depth reached 4.7 mm; then, an increase in the indentation force, accompanied with fluctuations, occurred. For the second indentation, a similar indentation–force curve located beneath that of the first indentation is observed. Thus, we conclude that the indentation force for the second indentation is lower than

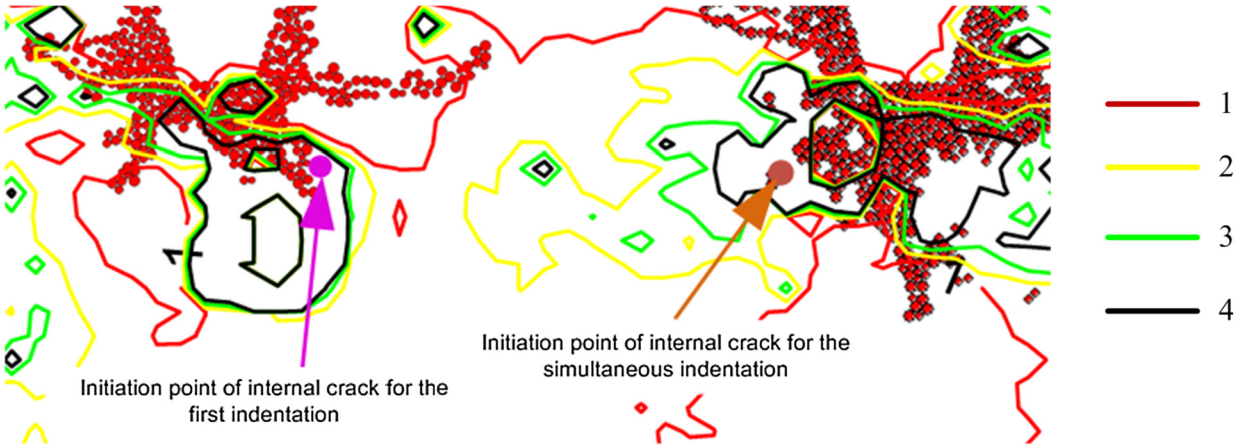

Fig. 13. The ratio of the horizontal stresses before internal crack initiation for simultaneous and sequential indentations.

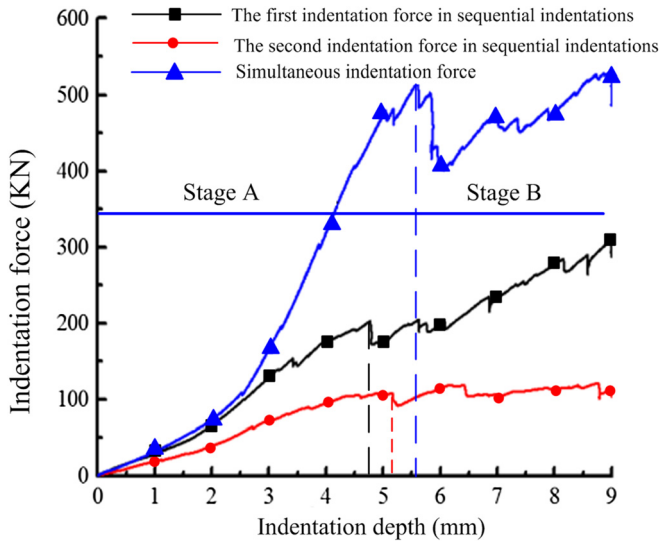

Fig. 14. Typical indentation forces: <sigma>2–<sigma>1 are 5 MPa–10 MPa.

that for the first indentation. This lower indentation force may result from the damage on the rock specimen and the change in the geometry of the sample caused by the first indentation. In addition, it is interesting to note that the crack initiation depths for sequential indentations were smaller than that for simultaneous indentations. Thus, in sequential indentations, cracks have more time to propagate for the same indentation depth.

Fig. 15 shows the consumed energies for various indentation tests, by integrating the indentation force and the indentation depth. Clearly, simultaneous indentations consumed more energy. According to the relation between indenter wear and the indentation force, these increased indentation energies for simultaneous indentations may result in more obvious tool wear. In addition, with the increase in spacing (Fig. 15(a)), indentation energy increased. For sequential indentations, the damage to rock specimens, caused by the first indentations, were similar for various spacings. However, the weakening effect of the first indentation on the second indentation force will decrease with the increase in spacing. Thus, for the same indentation depth, a larger spacing may result in more indentation energy for the second indentation. Similarly, for simultaneous indentations, the increase in spacing restrains the weakening effects of adjacent simultaneous indentations. Thus, the consumed energy will increase with the increase in spacing. In the second series of indentation tests, the indentation energy for sequential indentations approximately increased with the increase in differential stress. This phenomenon, reported by previous studies, may result from the increased <sigma>2 [16].

3.3. Indentation efficiency

The analysis of groove volumes, obtained by morphology measurements, indicates that larger grooves formed after sequential indentations (Fig. 16). These enlarged groove volumes may result from the more effective connections of internal

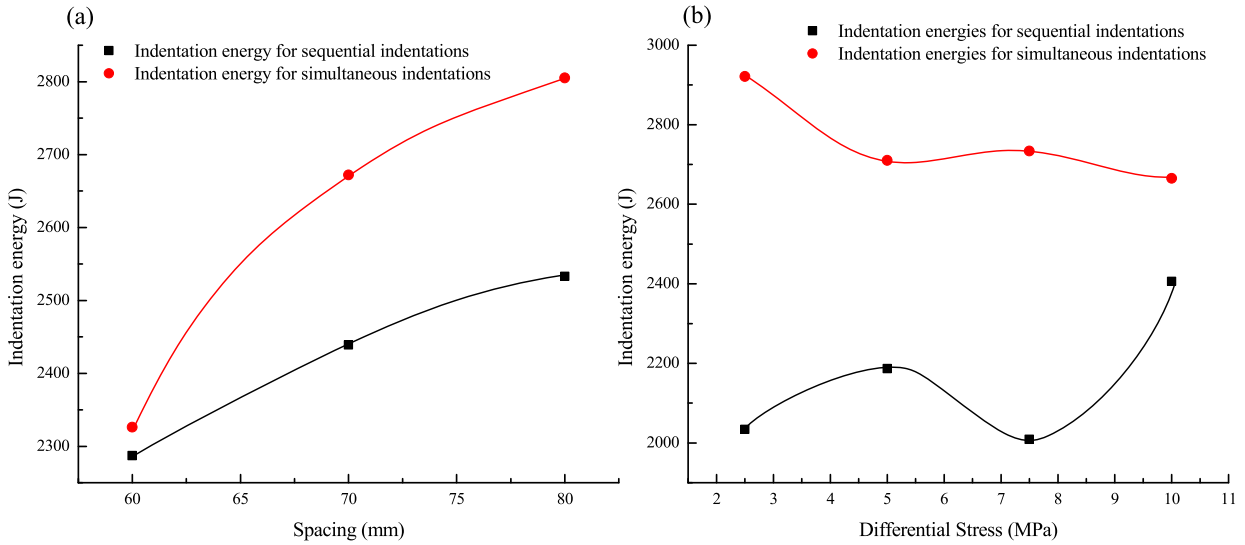

Fig. 15. Indentation energies: (a) indentation energies in the first series of tests; (b) indentation energies in the second series of tests.

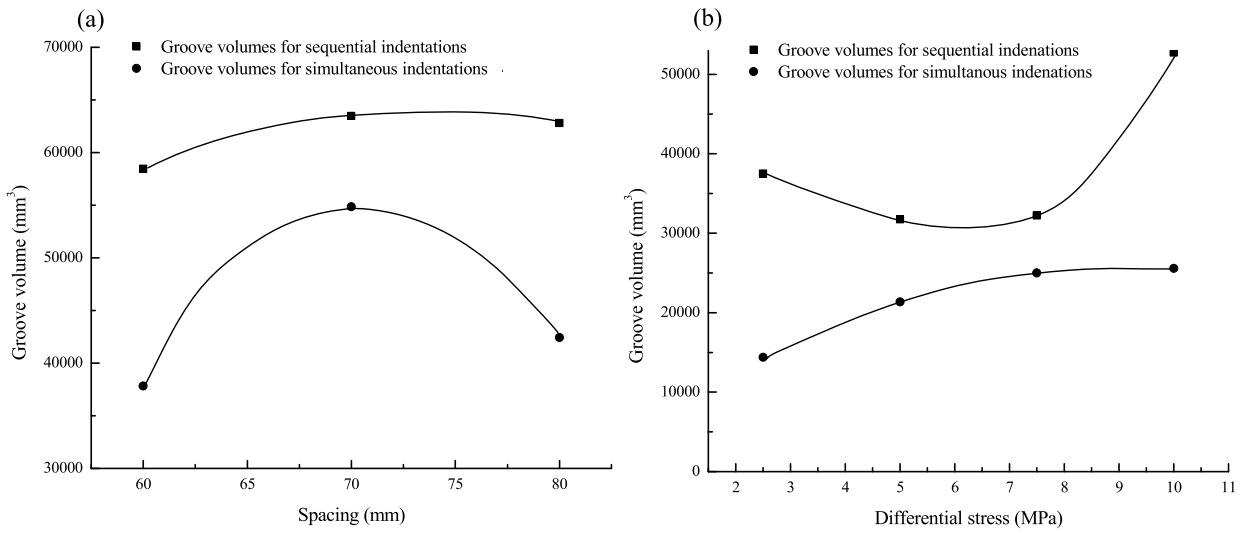

Fig. 16. Groove volumes: (a) groove volumes in the first series of tests; (b) groove volumes in the second series of tests.

cracks after sequential indentation. In addition, Fig. 16(a) indicates that the groove volume first increased and then decreased with the increase in spacing. This phenomenon may be reasonable, because overbreaking occurs for short spacings and results in relatively small groove. With the increase in spacing, moderate and insufficient rock breaking occur, and lead to a subsequent increase and decrease in the groove volume. This inference is properly validated by previous studies [29,30].

With the consumed energy in Fig. 15, Fig. 17 depicts the specific energy. First, the specific energy for sequential indentations was lower than that for simultaneous indentations. This decreased specific energy may result from the enlarged groove volumes and decreased indentation energy by sequential indentations. Thus, we can conclude that the sequential indentations instead of the simultaneous indentations lead to larger grooves with the same indentation energy. To form more chips with specific energy, we could apply sequential indentations; however, the wear degree of the first indenter may increase because of the relatively large indentation force. In addition, for simultaneous indentations in the first series of tests, the optimal spacing is about 70 mm; however, the specific energy for the sequential indentations slightly varied (Fig. 17(a)). Furthermore, with the increase in differential stress, the decrease in specific energy indicates that indentation efficiency increases; and this conclusion agrees well with previous studies [16].

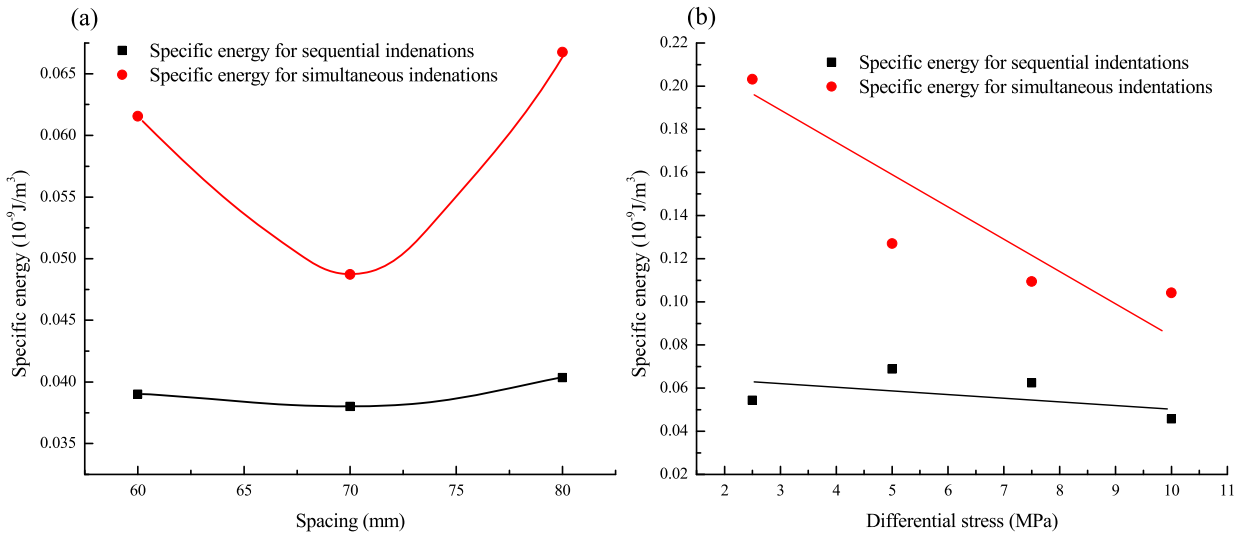

Fig. 17. Specific energies: (a) and (b) correspond to the first and second series of tests, respectively.

4. Conclusions

This article investigates the influence of the indentation sequence on rock breakages, indentation energy, and cutting efficiency by conducting laboratory and numerical indentation tests. First, laboratory tests indicate that sequential indentations instead of simultaneous indentations caused larger grooves, resulted from differences in crack propagation. In addition, the numerical study verified this conclusion by analyzing the stress condition in the indentation processes. For simultaneous indentations, two adjacent plastic zones were connected by only one internal crack, because the propagation of this internal crack restrained the propagation of the internal crack from the other inner rim. For sequential indentations, chips were formed by the connection of two internal cracks that initiated from adjacent plastic zones. Larger deflection angles, resulting in smaller chips, were observed in simultaneous indentations because of the increased compressive stress in the horizontal direction. Furthermore, an analysis of specific energy shows that sequential indentations occur instead of simultaneous indentations form larger grooves with the same indentation energy.

Acknowledgements

The authors would like to acknowledge these financial supports: the Doctoral Science Fund in the Hunan Institute of Engineering, the National Natural Science Foundation of China (Nos. 51774131, 51774132), the China Postdoctoral Science Foundation (2017M612557), and the Open Fund of the Safe Coal Mining Techniques in the Hunan University of Science and Technology (E21731), the Outstanding Youth Project (17B063) and the Pre-foundation for the National Science Foundation for China (YY1705) in the Hunan Institute of Engineering.

References

[1] H. Bejari, J. Khademi Hamidi, Simultaneous effects of joint spacing and orientation on TBM cutting efficiency in jointed rock masses, Rock Mech. Rock Eng. 46 (4) (2012) 897–907.
[2] Q.M. Gong, J. Zhao, Influence of rock brittleness on TBM penetration rate in Singapore granite, Tunn. Undergr. Space Technol. 22 (3) (2007) 317–324.
[3] H. Haeri, M.F. Marji, Simulating the crack propagation and cracks coalescence underneath TBM disc cutters, Arab. J. Geosci. 9 (2) (2016) 1–10.
[4] H.Y. Huang, E. Detournay, Intrinsic length scales in tool–rock interaction, Int. J. Geomech. 8 (2008) 39–44.
[5] Q. Liu, Y. Pan, J. Liu, X. Kong, K. Shi, Comparison and discussion on fragmentation behavior of soft rock in multi-indentation tests by a single TBM disc cutter, Tunn. Undergr. Space Technol. 57 (2016) 151–161.
[6] H. Huang, B. Damjanal, B. Detournay, Normal wedge indentation in rocks with lateral confinement, Rock Mech. Rock Eng. 31 (2) (1998) 81–94.
[7] Q.M. Gong, Y.Y. Jiao, J. Zhao, Numerical modeling of the effects of joint spacing on rock fragmentation by TBM cutters, Tunn. Undergr. Space Technol. 21 (1) (2006) 46–55.
[8] Q.M. Gong, J. Zhao, Y.Y. Jiao, Numerical modeling of the effects of joint orientation on rock fragmentation by TBM cutters, Tunn. Undergr. Space Technol. 20 (2005) 183–191.
[9] L.J. Yin, Q.M. Gong, H.S. Ma, J. Zhao, X.B. Zhao, Use of indentation tests to study the influence of confining stress on rock fragmentation by a TBM cutter, Int. J. Rock Mech. Min. Sci. 72 (2014) 261–276.
[10] N. Innaurato, C. Oggeri, P.P. Oreste, R. Vinai, Experimental and numerical studies on rock breaking with TBM tools under high stress confinement, Rock Mech. Rock Eng. 40 (5) (2007) 429–451.
[11] H.S. Ma, L.J. Yin, H.G. Ji, Numerical study of the effect of confining stress on rock fragmentation by TBM cutter, Int. J. Rock Mech. Min. Sci. 48 (2011) 1021–1033.
[12] T. Moon, J. Oh, A study of optimal rock-cutting conditions for hard rock TBM using the discrete element method, Rock Mech. Rock Eng. 45 (2011) 837–849.

[13] S.F. Zhai, X.P. Zhou, J. Bi, N. Xiao, The effects of joints on rock fragmentation by TBM cutters using General Particle Dynamics, Tunn. Undergr. Space Technol. 57 (2016) 162–172.
[14] X. Zhu, W. Liu, X. He, The investigation of rock indentation simulation based on discrete element method, KSCE J. Civ. Eng. (2016), https://doi.org/10.1007/s12205-016-0033-4.
[15] J. Liu, P. Cao, K.H. Li, A study on isotropic rock breaking with TBM cutters under different confining stresses, Geotech. Geolog. Eng. 33 (6) (2015) 1379–1394.
[16] J. Liu, P. Cao, D.Y. Han, Sequential indentation tests to investigate the influence of confining stress on rock breakage by tunnel boring machine cutter in a biaxial state, Rock Mech. Rock Eng. 49 (2016) 1479–1495.
[17] S. Yagiz, Assessment of brittleness using rock strength and density with punch penetration test, Tunn. Undergr. Space Technol. 24 (2009) 66–74.
[18] Y. Chen, P. Cao, R. Chen, Effect of water–rock interaction on the morphology of a rock surface, Int. J. Rock Mech. Min. Sci. 47 (2010) 816–822.
[19] Y.L. Zhao, L.Y. Zhang, W.J. Wang, J.Z. Tang, H. Lin, W. Wan, Transient pulse test and morphological analysis of single rock fractures, Int. J. Rock Mech. Min. Sci. 91 (2017) 139–154.
[20] L. Scholtès, F.V. Donzé, A DEM analysis of step-path failure in jointed rock slopes, C. R., Mecanique 343 (2015) 155–165.
[21] Y. Xie, P. Cao, J. Liu, L. Dong, Influence of crack surface friction on crack initiation and propagation: a numerical investigation based on extended finite element method, Comput. Geotech. 74 (2016) 1–14.
[22] Itasca Consulting Group, Users' manual for particle flow code in 2 dimensions (PFC2D). Version 3.1, Minneapolis, Minnesota, 2002.
[23] X.P. Zhang, Q. Liu, S. Wu, X. Tang, Crack coalescence between two non-parallel flaws in rock-like material under uniaxial compression, Eng. Geol. 199 (2015) 74–90.
[24] J. Liu, P. Cao, Z. Jiang, Y.L. Zhao, R.H. Cao, Numerical simulation on effects of embedded crack on rock fragmentation by a tunnel boring machine cutter, J. Cent. South Univ. 21 (2014) 3302–3308.
[25] Y. Zhao, L. Zhang, W. Wang, C.Z. Pu, W. Wan, J. Tang, Cracking and stress–strain behavior of rock-like material containing two flaws under uniaxial compression, Rock Mech. Rock Eng. 49 (7) (2016) 2665–2687.
[26] J. Bi, X.P. Zhou, Q.H. Qian, The 3D numerical simulation for the propagation process of multiple pre-existing flaws in rock-like materials subjected to biaxial compressive loads, Rock Mech. Rock Eng. 49 (5) (2015) 1611–1627.
[27] T. Moon, M. Nakagawa, J. Berger, Measurement of fracture toughness using the distinct element method, Int. J. Rock Mech. Min. Sci. 44 (2007) 449–456.
[28] S.Y. Li, T.M. He, X.C. Yin, Introduction of Rock Fracture Mechanics, Press of Chinese University of Science and Technology, Hefei, 2010, pp. 157–169 (in Chinese).
[29] J.W. Cho, S. Jeon, H.Y. Jeong, S.H. Chang, Evaluation of cutting efficiency during TBM disc cutter excavation within a Korean granitic rock using linear-cutting-machine testing and photogrammetric measurement, Tunn. Undergr. Space Technol. 35 (2013) 37–54.
[30] J. Liu, P. Cao, D.Y. Han, The influence of confining stress on optimum spacing of TBM cutters for cutting granite, Int. J. Rock Mech. Min. Sci. 88 (2016) 165–174.